ACS ENVIRONMENTAL Au
AN OPEN ACCESS JOURNAL OF THE AMERICAN CHEMICAL SOCIETY

pubs.acs.org/environau
Article

Silver-Doped Porous Copper Catalysts for Efficient Resource Utilization of CO-Containing Flue Gases

Zhengkai Zhuang, Guangtao Wang, Wen Zhao, Ruixin Yang, Yilin Zhou, and Wenlei Zhu*

Cite This: ACS Environ. Au 2025, 5, 287−297
Read Online

ACCESS | Metrics & More | Article Recommendations | Supporting Information

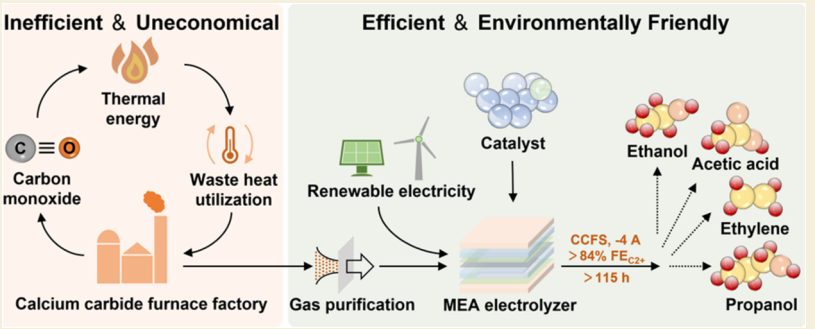

ABSTRACT: CO is both a key intermediate in the electrocatalytic conversion of CO_2 and a valuable C_1 resource, with the potential to reduce carbon emissions and mitigate the energy crisis. However, industrially emitted CO remains underutilized due to inefficiencies and economic challenges. Electrocatalytic CO reduction offers a promising approach for the efficient and environmentally friendly utilization of CO-containing flue gases. Nevertheless, current technologies face limitations, such as low operating currents and difficulties in adaptation to complex reaction gas components. Here, we report a low-cost silver-doped porous copper oxide (Ag-pCuO) catalyst. The doping of a moderate amount of Ag (0.875% doping) endows porous CuO with highly selective Cu−Ag active sites, enhanced CO adsorption, and improved surface valence stability, allowing $Ag_{0.875\%}$-pCuO to achieve remarkable catalytic performance in a carbon-doped titanium-based membrane electrode assembly electrolytic cell. It achieves a remarkable C_{2+} faradic efficiency of up to 94% at a high current density of −4 A under a simulated calcium carbide furnace gas atmosphere and demonstrates exceptional stability, with only a 6.08% decline in C_{2+} faradic efficiency after over 110 h of continuous operation. In summary, this research presents a novel approach for applying Ag-doped copper-based catalysts to industrially utilize CO-containing flue gases, especially from calcium carbide furnaces.

KEYWORDS: *electrocatalytic, flue gas, resource utilization, CO reduction, electrolyzer*

INTRODUCTION

As a major greenhouse gas, CO_2 is a key target for mitigating climate change and the greenhouse effect, as well as a cheap, abundant, and nontoxic C_1 resource.[1,2] Electrocatalytic CO_2 reduction reaction (CO_2RR) as a green and industrialized potential technology has contributed significantly to the process of achieving carbon neutrality goals.[3−9] However, the CO_2RR faces efficiency losses due to the formation of HCO_3^-/CO_3^{2-} in strongly alkaline environments, which inhibits hydrogen precipitation reactions and lowers C_{2+} product conversion efficiency. Recent advances have been achieved in a two-step strategy, where CO_2 is first reduced to CO and then efficiently converted electrocatalytically to C_{2+} products.[10−12] Employing CO as an intermediate product in CO_2RR enhances the overall efficiency of C_{2+} conversion and lowers operating costs.[13−15] Advancing research in electrocatalytic CO reduction (CORR) could enable the green and efficient utilization of CO_2 while also helping to mitigate climate change and the energy crisis.[11] However, CORR remains at the laboratory stage due to the high cost of industrial CO production and the low efficiency of catalysts at the industrial scale.[16]

As a key renewable C_1 feedstock for industrial chemical production, CO can be sourced from various industrial methods and is also found in the flue gases of many industries. For instance, calcium carbide furnace gas (CCFS), coke oven gas, and yellow phosphorus flue gas contain significant amounts of CO, with concentrations in CCFS and yellow phosphorus flue gas exceeding 80%.[17,18] However, despite their high potential for resource recovery, industrial waste gases are

Received: October 31, 2024
Revised: February 19, 2025
Accepted: February 19, 2025
Published: March 3, 2025

not efficiently utilized. Instead, they are either purified and discharged directly or undergo CO_2 capture and sequestration following secondary incineration.[19] Direct discharge raises atmospheric CO to levels that can be harmful to human health, while CO_2 capture and sequestration increase treatment costs and may lead to higher carbon emissions. Cyclone dedusting and modified activated carbon adsorption now enable the removal of dust and catalyst-poisoning gases from exhaust streams.[20] Therefore, using CO-containing industrial flue gases as a source for the CORR lowers both the feedstock costs and the environmental impact associated with industrial emissions.

Currently, the CORR typically utilizes only analytically pure CO (99.99%) for laboratory-scale studies.[21−24] A subset of materials capable of obtaining C_{2+} faradic efficiencies greater than 80% ($FE_{C_{2+}}$ > 80%) are often realized only at low current density. For instance, Bao et al. reported C_{2+} faradic efficiencies (FE) exceeding 90% using copper single atoms at a current density of −32 mA cm^{-2};[25] similarly, Li et al. achieved $FE_{C_{2+}}$ greater than 95% at a lower current density of −90 mA cm^{-2} with diatomic copper sites.[26] While these materials demonstrate excellent CORR selectivity, their performance is limited by low operating currents, which poses challenges for practical applications beyond the laboratory. Techno-economic analyses (TEAs) indicate that a profitable CORR system requires a reaction rate exceeding 100 mA cm^{-2}.[14] In contrast, materials capable of stable operation at high currents can achieve only low $FE_{C_{2+}}$. For instance, Guan et al. reported a $FE_{C_{2+}}$ of approximately 60% using a Cu−Au alloy at a high current density of −217 mA cm^{-2}.[27] Luc et al. achieved only 76% C_{2+} faradic efficiency at a higher current density of −300 mA cm^{-2} with two-dimensional (2D) copper nanosheets.[28] In summary, there is an urgent need to develop a low-cost catalyst that can withstand high currents for extended periods without performance degradation in a nonanalytically pure CO atmosphere, thereby enhancing the utilization of CORR for treating CO-containing flue gases.

Copper-based catalysts are the only class capable of electrocatalytic reduction of CO to C_{2+} products.[10,29−32] They are primarily doped and structurally modulated with noble metals to enhance the C_{2+} selectivity and stability. Among these methods, structural modulation is relatively inexpensive but tends to exhibit poor catalytic efficiency and stability. Zhuang et al. achieved a 70% $FE_{C_{2+}}$ at −40 mA cm^{-2} using open nanocavity Cu but could only operate stably for 2.5 h at −0.56 V.[33] In contrast, noble metal doping, featured by more controllable synthesis and superior C_{2+} production efficiency, has emerged as the predominant method for modulating copper-based catalysts.[34] Wang et al. achieved an $FE_{C_{2+}}$ exceeding 90% using Ag−Ru−Cu at a current density of −(300−600) mA cm^{-2}, maintaining stable operation for 100 h at a total current of −1.5 A.[1] Long et al. obtained a $FE_{C_{2+}}$ higher than 80% at −500 mA cm^{-2} using CuO-Au, but the material was only capable of stable and efficient operation for 8 h at −0.58 V.[35] Dorakhan et al. achieved $FE_{C_{2+}}$ greater than 75% at −300 mA cm^{-2} using Ag−Cu_2O, maintaining stable and efficient operation for 17 h at −100 mA cm^{-2}.[36] Additional examples of precious metal doping are presented in Table S2. Catalysts doped with Ag typically exhibit superior catalytic performance at high currents, and Ag is less expensive than other high-value-added precious metals. Therefore, this study focuses on doping with Ag; however, only a moderate loading of Ag effectively promotes *CO coverage on the catalyst and creates stable Cu−Ag active sites with efficient C_{2+} selectivity.[36−38] Thus, optimizing the Ag loading ratio is crucial for developing a copper-based CORR catalyst suitable for treating CO-containing flue gases.

In this research, we demonstrated an $Ag_{x\%}$-pCuO compound with a porous structure and uniformly doped with a small amount of Ag as a CORR catalyst with high C_{2+} selectivity at high currents, showing remarkable potential for efficiently utilizing CCFS. In performance tests, the membrane electrode assembly (MEA) electrolysis cell was chosen over traditional H cells and flow cells due to its simpler structure, higher mass transfer efficiency, and closer alignment with industrial production. The simulated gas from the CCFS, which has the highest CO concentration among industrial flue gases, served as the gas source for the CORR reaction. Subsequently, a chronopotentiometry test of the materials was carried out in the test environment described above, with $Ag_{0.875\%}$-pCuO (the actual Ag in the material is approximately 0.87% based on ICP testing results) at the optimal ratio of Ag:Cu was able to obtain a C_{2+} faradic efficiency of 94% at a high current of −4 A and was only able to attenuate the C_{2+} faradic efficiency by 6.08% after more than 110 h of stable operation. In comparison, the $Ag_{0.875\%}$-pCuO significantly outperformed the pCuO without Ag doping ($FE_{C_{2+}}$ = 40%, 4 h) in terms of treatment efficiency for simulated flue gas. Additionally, it does not require high-value precious metals such as Au, thereby lowering catalyst costs. It shows promising application potential for treating CCFS and other CO-containing flue gases such as yellow phosphorus flue gas, carbon black flue gas, and blast furnace gas.

EXPERIMENTAL METHODS

Materials

$CuSO_4·5H_2O$ (AR), $Cu(NO_3)_2$ (AR), aqueous $NH_3·H_2O$ solution (AR), $AgNO_3$ (AR), NaOH (AR), KOH (AR), Nafion 212 and 5% Nafion perfluorinated resin solution 5 wt % (D520, EW = 1,000), deuterated water (D_2O), dimethyl sulfoxide (DMSO), isopropanol (AR), CO (grade 4), and simulated CCFS (85%CO, 10%CO_2, 5% N_2) were purchased from Nanjing Tianze. The carbon-based gas diffusion electrode (GDE; Sinero 39BB), anion exchange membrane (PiperION, Versogen A40-HCO_3), and ultrapure water (18.2 MΩ; prepared by the Milli-Q pure water meter) were used in all of the experiments.

Synthesis and Characterization of Ag-Doped Porous CuO

The synthesis of Ag-pCuO catalysts was performed following a two-step procedure. The first step, which is the synthesis of pCuO nanoparticles (NPs), is modified and optimized from the previously reported method. $Cu(NO_3)_2$ (1 g) was dissolved in 100 mL ultrapure water and vigorously stirred at room temperature. Next, 30 mL of an aqueous solution of $NH_3·H_2O$ (0.150 M) was added to the mixed solution. Additionally, NaOH (1 M) was slowly added to the mixed solution at a titration rate of 2 mL min^{-1} to adjust the pH in the mixed solution to 9−10 for the precipitation of $Cu(OH)_2$. The mixed solution was then vigorously stirred for half an hour. The reaction mixture was then centrifuged and washed three times with ultrapure water to obtain porous pCuO Nps precursors. And then pCuO Nps precursors were dried under vacuum at 60 °C for one night. Ultimately, the dried copper hydroxide nanorods were annealed at 500 °C for 2 h under a static air atmosphere at a ramp rate of 32 °C per minute.

Ag doping is achieved by using the chelating effect of sodium citrate to link Ag^+ on the surface of CuO and its reducing property to

https://doi.org/10.1021/acsenvironau.4c00121
ACS Environ. Au 2025, 5, 287−297

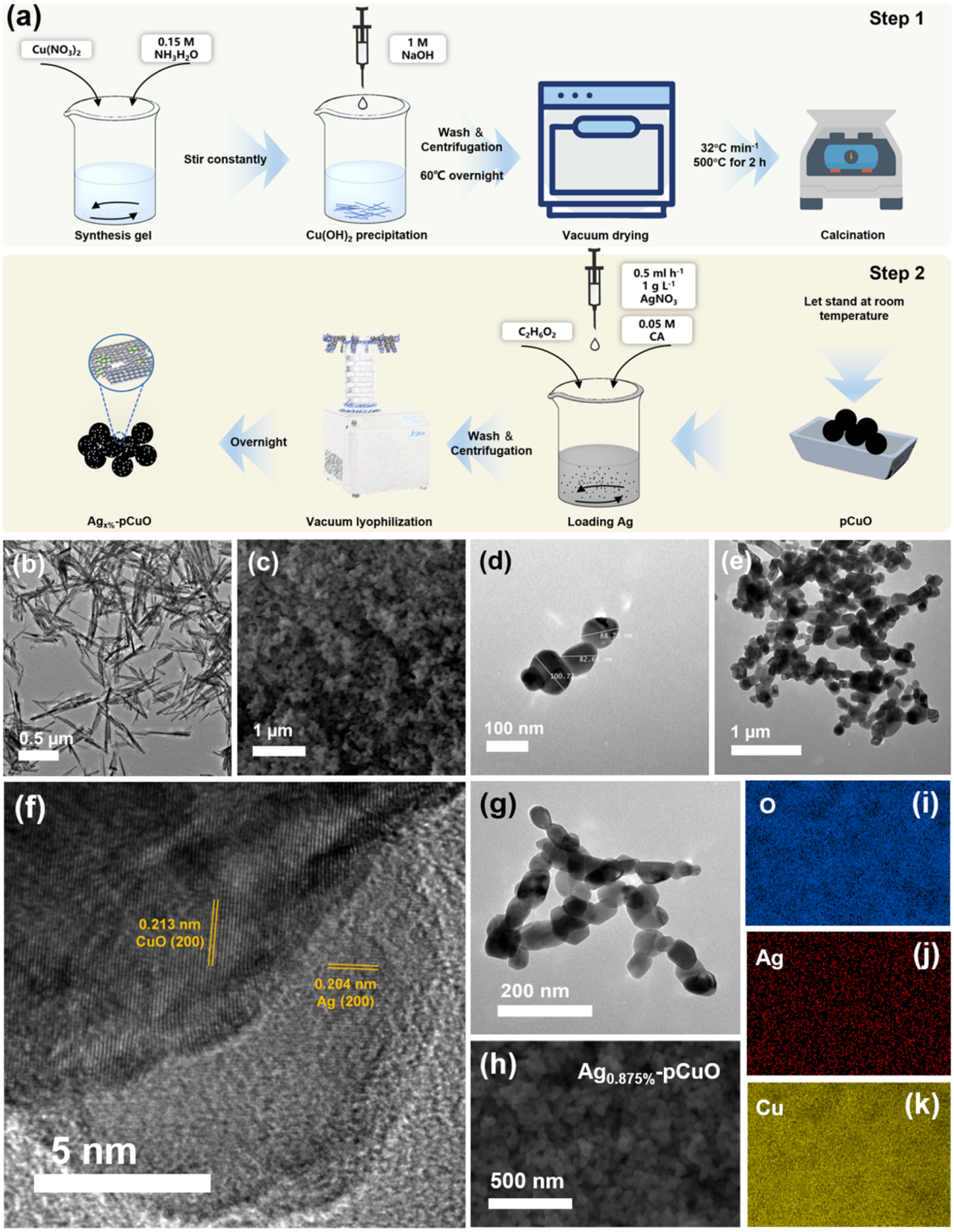

Figure 1. Preparation methods and characterization of $Ag_{x\%}$-pCuO, pCuO, and $Cu(OH)_2$ needles. (a) Schematic illustration of the preparation of $Ag_{x\%}$-pCuO, (b) TEM images of $Cu(OH)_2$ needles, (c) SEM images of $Ag_{0.875\%}$-pCuO, (d, g) TEM images of $Ag_{0.875\%}$-pCuO, (e) TEM images of pCuO, (f) high-resolution TEM (HR-TEM) images of $Ag_{0.875\%}$-pCuO, and (h−k) element mapping analyses of $Ag_{0.875\%}$-pCuO.

bind Ag^+ to Ag^0, ultimately achieving a uniform distribution of Ag on the surface of CuO. First, 1 mL of sodium citrate solution (0.05 mol L^{-1}) was taken and added to 20 mL of ethylene glycol solution with continuous stirring; then, 100 mg of pCuO powder was homogeneously dispersed in the continuously stirred ethylene glycol solution. After 5 min, 0.875 mL of silver nitrate solution (1 mg mL^{-1}) was slowly dropped into (0.5 mL h^{-1}) the beaker with continuous vigorous stirring. Then, the catalyst was stirred vigorously for 30 min. The catalyst was washed twice by centrifugation with ethanol and ultrapure water, respectively, and then lyophilized, and finally, the $Ag_{0.875\%}$-pCuO catalyst was obtained. Other $Ag_{x\%}$-pCuO catalysts were also prepared using the same preparation method as above except that the amount of silver nitrate solution added must correspond to the composition of the final material.

Characterization

The approximate morphological characteristics and elemental composition of $Ag_{x\%}$-pCuO and pCuO will be determined by scanning electron microscopy (SEM, QUANTA200) as well as energy-dispersive spectrometry (EDS mapping). At the same time, the

https://doi.org/10.1021/acsenvironau.4c00121
ACS Environ. Au 2025, 5, 287−297

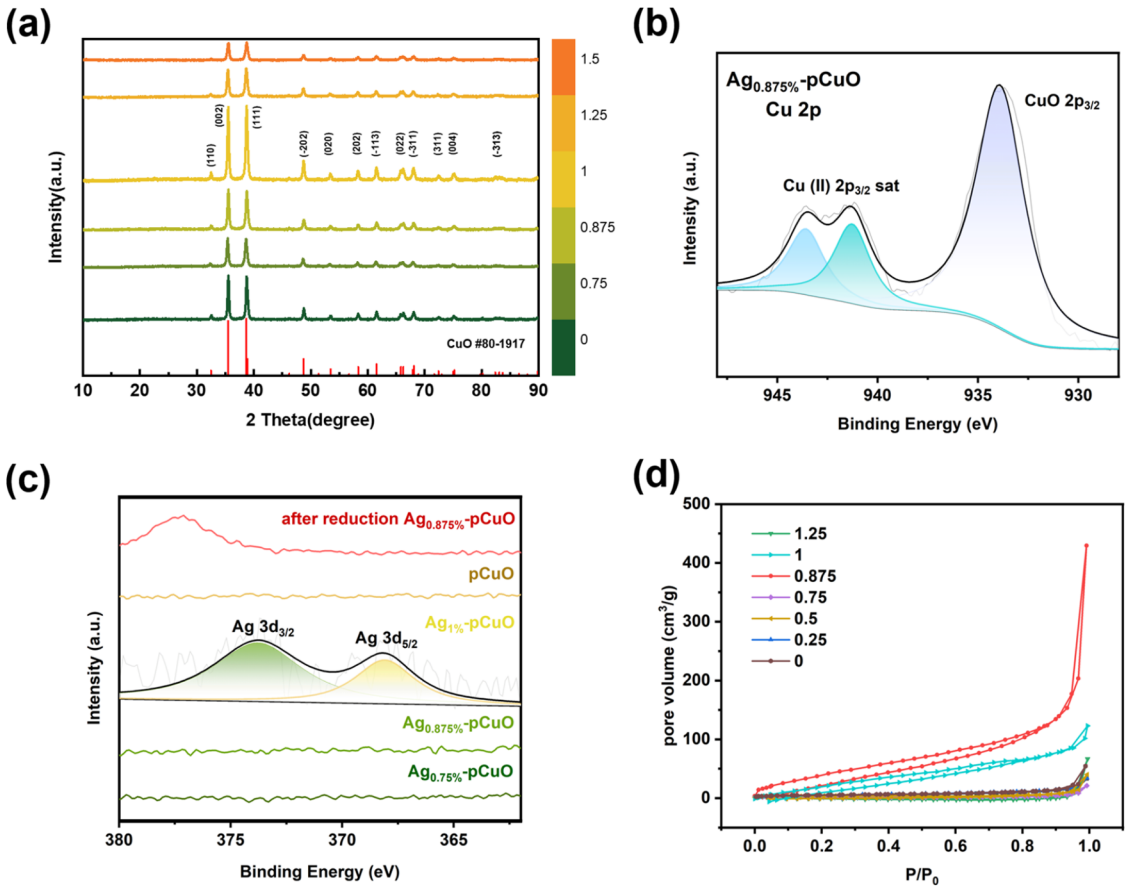

Figure 2. Structural characterizations of the Ag-pCuO series and pCuO. (a) XRD patterns of Ag-pCuO series and pCuO, (b) Cu 2p spectra of $Ag_{0.875\%}$-pCuO, (c) Ag 3d spectra of Ag-pCuO series and pCuO, and (d) specific surface area measurement of Ag-pCuO series and pCuO.

size of the material and its microstructure will also be characterized in more detail by electron transmission microscopy (TEM, JEM-2800). In addition, the crystal structure of the material and its components were analyzed by powder X-ray diffraction (XRD, Shimadzu). Then, the composition and valence changes of the elements on the catalyst before and after the reaction were probed by X-ray photoelectron spectroscopy (XPS, PHI5000 Versaprobe). Considering that the catalyst is difficult to remove from the carbon paper after the electrocatalytic reduction reaction, our team performed XPS tests directly on the entire catalyst-loaded carbon paper. In this case, the sampling method was to dry the tested carbon paper at room temperature for 9 h and then cut the carbon paper to 0.5 × 0.5 cm^2. Next, the specific surface area of the material was measured in this study by the Brunauer–Emmett–Teller (BET) test. Finally, in order to investigate the actual loading of Ag on CuO, this study quantitatively analyzed the exact amount of each element in the material by inductively coupled plasma mass spectrometry (ICP, 7400 ICP-OES).

Electrochemical CO Reduction Measurement

The electrochemical properties of all samples in this experiment were tested by MEA in DH7002A and RU-FT30120 electrochemical workstations. The MEA was assembled by stacking the gas diffusion electrodes (GDE), anion exchange membrane (AEM), and IrO_2–Ti felt and pressing them between the cathode plate (25 cm^2 flow field, titanium) and the anode plate (25 cm^2 flow field, titanium). In this case, GDE was prepared by spraying the catalyst ink (30 mg sample, 2970 μL of isopropanol, 30 μL of Nafion) uniformly onto the hydrophobic gaseous diffusion layer by a spray gun technique to obtain a catalyst with an average of 0.48 mg cm^{-2}. KOH (1 M) solution was used as the electrolyte in the anode of MEA and was delivered with a peristaltic pump (5 mL min^{-1}). In addition, the gas flow of CO was maintained at 40 sccm during the electrochemical tests. The FE for the products was calculated using the following equation:

$$\mathrm{FE}\ (\%) = nFxV \times 100 j_{\mathrm{Tot}}^{-1}$$

$FE_{C_{2+}}$ is the calculated FE for C_{2+} in percentage.

Product Analysis

The electrochemical properties of all samples were tested by using the chronopotentiometry test. In addition, the collection of both liquid and vapor phase products in the test was carried out after activation for 20 min at the start of the test. The gas-phase products were detected by an Agilent 7890B gas chromatograph (GC) (equipped with a 5 Å molecular sieve column, TDX-01 column, thermal conductivity detector, and flame ionization detector). While the liquid-phase products were quantitatively and qualitatively detected by 400 MHz nuclear magnetic resonance (NMR).

In Situ Characterization

In order to investigate in depth the mechanism of trace-doped Ag in improving the catalytic performance of pCuO in CORR, our team used in situ Raman (LabRAM RH Evolution) to monitor the intermediate species on the surface of the material at different potentials in real time during the material's CORR process.

Application Scene

Considering the higher purity of CO (>80%) contained in the CCFS (Table S1), it is possible to reduce the cost of CO purification prior to resource utilization and improve the feasibility and economics of flue gas resource utilization.[39] The application scenario simulated in this experiment is the electrocatalytic utilization of the flue gas from a calcium carbide furnace after preliminary dedusting and purification. Currently, CCFS contains a portion of gaseous impurities (HCN, COS, and H_2S) and solid impurities (dust), which tend to poison the

https://doi.org/10.1021/acsenvironau.4c00121
ACS Environ. Au 2025, 5, 287–297

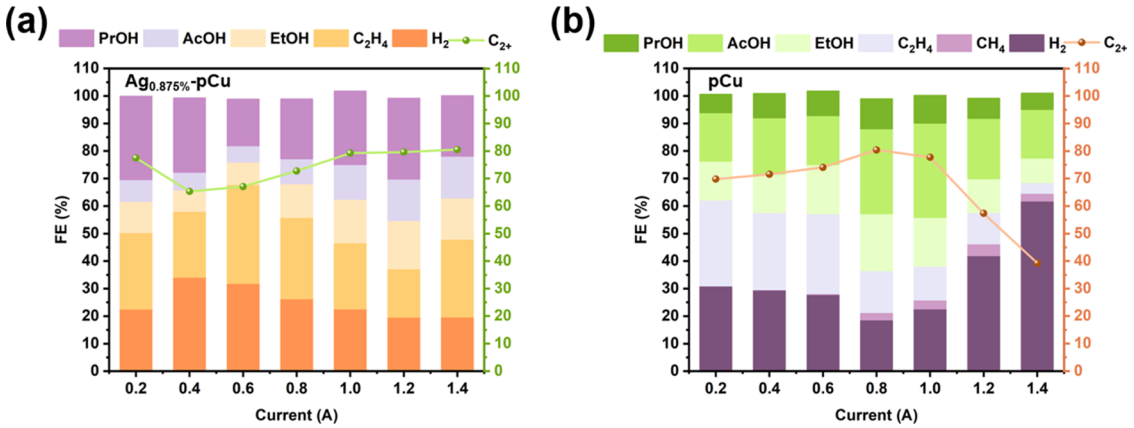

Figure 3. Lab-scale measurement of Ag-pCuO series' electrocatalytic CORR performances. Faradic efficiency of the reduction products for (a) $Ag_{0.875\%}$-pCuO and (b) pCuO at different applied currents.

catalyst.[40] The former can be removed by adsorption[41] and catalytic oxidation,[42] while the latter can be removed by means of bag dedusting or cyclone dedusting. Therefore, in this study, the CCFS fraction with the above impurities and H_2 removed (to avoid confusion between the H_2 in the simulated CCFS and the H_2 in the product) was used as the gas fraction of the simulated CCFS in the pilot test (85% CO, 10% CO_2, 5% N_2, Nanjing Tianze Gas Co., Ltd.). Then, the CORR performance and catalytic stability of the different catalysts were compared to each other at high currents to select the best catalyst for the electrocatalytic reduction of the dedusted flue gas from the calcium carbide furnace.

RESULTS AND DISCUSSION

Characterization of Ag-Doped Porous CuO

Initially, Dorakhan et al. found that the Ag:Cu ratio on the catalyst surface was the key factor affecting the performance of the catalyst.[36] To this end, in this study, a porous CuO (pCuO) was synthesized with a 62% C_{2+} product selectivity in the electrocatalytic reduction of CO_2, referring to a previous report. The following are the results of our team's characterization of the catalyst (named $Ag_{x\%}$-pCuO, with x% representing the mass ratio of Ag:Cu during the preparation process) using a series of non-in situ characterizations at different Ag doping levels. In this manuscript, it was found that the overall structure of pCuO exhibits a reticulated porous structure, which consists of many cross-linked CuO nanorod-like particles, and most of these nanoparticles (average size 70.99 nm, Figure S3), which are relatively smooth in appearance, do not exist as individual nanoparticles but rather as multiple particles cross-linked into a reticulated structure (Figures 1b−d and S1a−g). The formation of this structure is due to the precursor being an acicular $Cu(OH)_2$ precipitate (Figure 1b), and the stacking structure of this elongated acicular material is similar to the interwoven structure between the carbon fibers in a carbon cloth capable of forming a porous nanonetwork upon calcination, an essential property required to increase the efficiency of the gas product detachment in high-efficiency CORR.[43] Then, in this study, the chelating and reducing properties of sodium citrate and ethylene glycol were utilized to couple Ag^+ with pCuO and reduce Ag^+(Figure 1a),[44] which in turn resulted in uniformly loaded pCuO with Ag. From the EDS images, it can be concluded that when the Ag doping amount is less than 1%, the reduced Ag is uniformly distributed on the surface of the pCuO support, and the Ag loading on the pCuO surface is directly proportional to the doping amount in the prepared material. This implies that the Ag:Cu ratio of the catalyst can be modulated by the synthesis method of this experiment (Figures 1h−k, S2, and Table S3). Combined with the results of BET (Figure 2d), the research found that when the negative doping of Ag is less than 1%, there is not much difference in the structure, size, and surface morphology of the material before and after loading, which indicates that a small amount of Ag doping does not destroy the basic morphology of CuO (Figures 1d,e,g and S1b,d). When the doping amount of Ag is greater than 1%, Ag starts aggregating on the CuO surface to form AgNps and becomes unevenly distributed (Figures 1f and S1h), which will block the pore size of pCuO to a certain extent, reducing the specific surface area of the material (Table S4) and affecting to a certain extent the dominant active site of the material in CORR, which in turn changes the catalytic selectivity of the material.[45]

However, the maximum doping of Ag in this material is only 1.25%, which makes none of the metallic peaks of Ag appear in the XRD images of $Ag_{x\%}$-pCuO (Figure 2a). This also means that sodium citrate only reduces Ag^+ but not CuO during the preparation of the material, and the main composition and crystal structure of the material is still dominated by CuO. Thus, in this research, the valence information on the elements on $Ag_{x\%}$-pCuO was deeply probed by XPS, and it was found that the Cu valence on the material surface at different Ag doping levels was basically Cu^{2+}, which was consistent with the previous XRD results. As for the valence state of Ag on the surface of the material, two strong binding energy peaks (367.9 eV: Ag $3d_{5/2}$, 374.27 eV: Ag $3d_{3/2}$) were observed only on $Ag_{1\%}$-pCuO with higher Ag doping. Considering that the content of Ag on the surface of the material may be lower than the detection limit of XPS, in this research, we believe that the valence state of Ag on the surface of the material at other doping levels is consistent with that of Ag^0 (Figures 2b,c, S4 and S5). $Ag_{1\%}$-pCuO is consistent with Ag^0 (Figure 2c). BET tests further demonstrated that $Ag_{0.875\%}$-pCuO possesses the largest specific surface area. This result stems from the doping of low concentrations of Ag, which introduces new meso- and microporous structures into the pCuO system, reducing the average pore size of $Ag_{0.875\%}$-pCuO compared to pCuO and effectively increasing the material's specific surface area. (Figure 2d and Table S4).

Next, the team used flow cells to evaluate the CORR performance of $Ag_{x\%}$-pCuO and pCuO in a 1 M KOH solution

https://doi.org/10.1021/acsenvironau.4c00121
ACS Environ. Au 2025, 5, 287−297

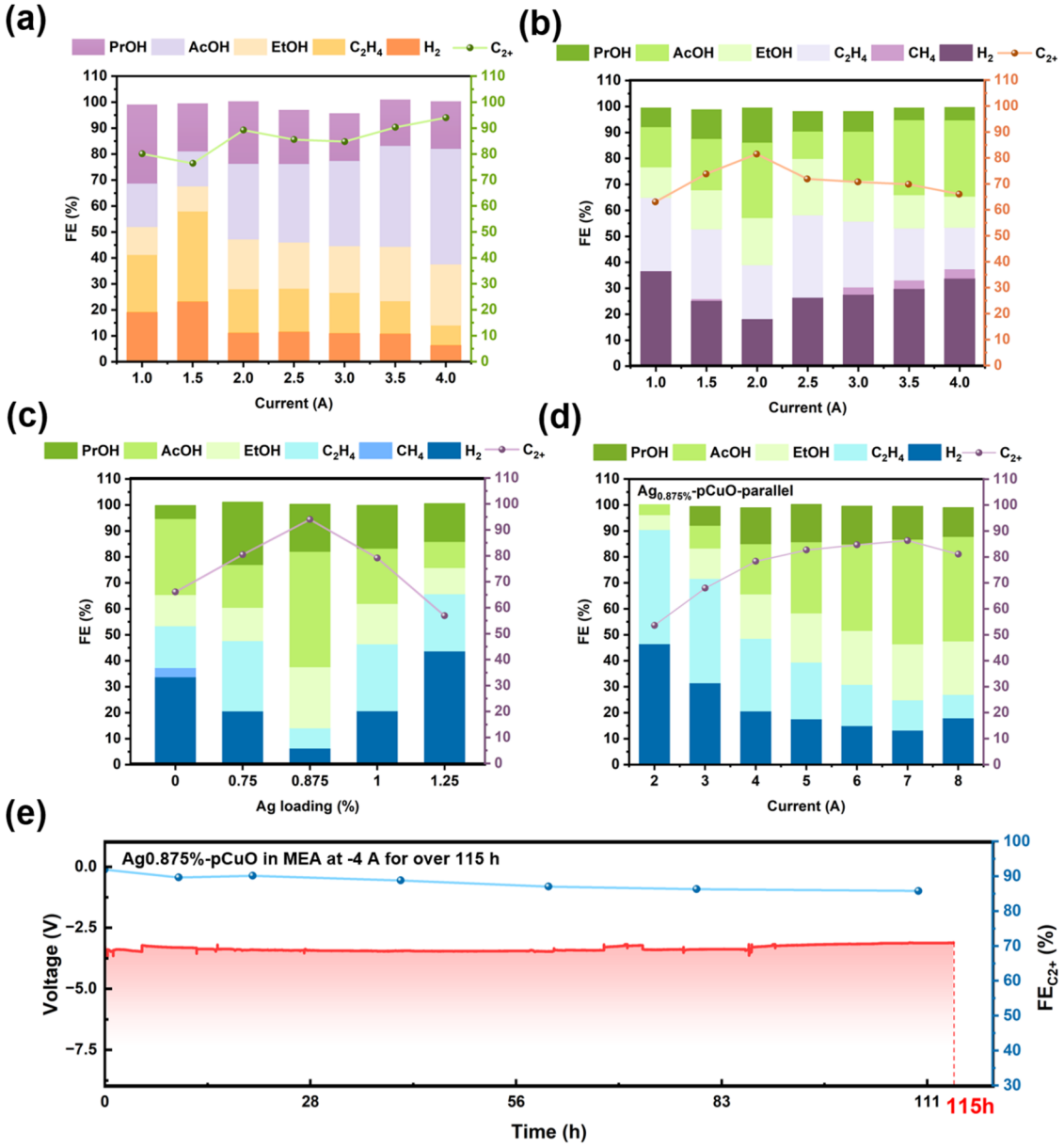

Figure 4. Pilot test of Ag-pCuO series' electrocatalytic CORR performances. FE distribution of the CORR products for the (a) $Ag_{0.875\%}$-pCuO and (b) pCuO catalyst at different currents in an MEA cell, (c) comparison of the electrocatalytic performances of Ag-pCuO series and pCuO at −4 A, and (d) FE distribution of the CORR products for the $Ag_{0.875\%}$-pCuO at different currents in a reaction system with two cells in parallel. The gas source of all of the tests is simulated CCFS and (e) chronopotentiometry stability test of $Ag_{0.875\%}$-pCuO at −4 A (−111.11 mA cm^{-2}) in MEA.

to make a preliminary judgment on the potential of each material for the treatment of simulated CCFS. In this research, chronopotentiometry test was carried out for each material at different operating currents, as shown in Figure 3b. The optimum applied current for pCuO was −0.8 A, and $FE_{C_{2+}}$ up to 81.4% was obtained at this operating current. However, the CORR performance of pCuO decreases rapidly with increasing current, and pCuO is able to obtain only 38.25% of $FE_{C_{2+}}$ when the applied current is −1.4 A, which makes it difficult for pCuO to be competent for industrial production. And the CORR performance of Ag-doped pCuO is shown in Figure 3a, where $Ag_{0.875\%}$-pCuO is able to obtain a peak C_{2+} faradic efficiency of 80.5% when the applied current reaches −1.4 A, and the $FE_{C_{2+}}$ of $Ag_{0.875\%}$-pCuO has been increasing from 66% to 80.5% from the beginning to the end of −1.4 A, which suggests that the $Ag_{0.875\%}$-pCuO has the potential for stable and efficient C_{2+} production at high currents. In addition, $Ag_{0.875\%}$-pCuO possessed the highest $FE_{C_{2+}}$ at a high current of −1.4 A compared to other catalysts at Ag doping (Figure S6), which could be attributed to its superior specific surface area and suitable Cu, Ag, and Cu−Ag active sites.

Application Scene

A material that can operate stably and efficiently under high currents is important for its ability to be widely used in industry.[46] In order to investigate the material in high-current operation and its potential in treating CO-containing flue gases, the team conducted medium-scale experiments on $Ag_{x\%}$-pCuO under simulated CCFS. In this research, the previous flow cell and pure CO atmosphere were still used, but the applied current increased from −1.4 to −4 A. It was found that

https://doi.org/10.1021/acsenvironau.4c00121
ACS Environ. Au 2025, 5, 287−297

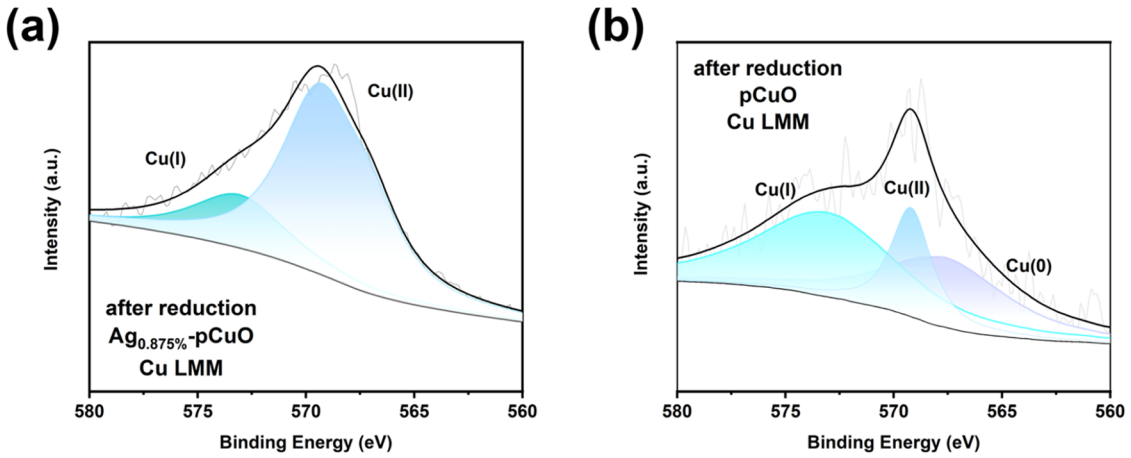

Figure 5. Auger patterns (a) of $Ag_{0.875\%}$-pCuO materials after the 110 h CORR reaction and Auger patterns (b) of Ag-pCuO materials after the 4.5 h CORR reaction.

the hydrogen precipitation of the material under high current increased significantly due to the disadvantages of the flow cell in mass transfer and heat dissipation. When the current applied to the cell reaches −3.5 A, the FE_{H2} of $Ag_{0.875\%}$-pCuO rises to 42.7%, while at the same time, the $FE_{C_{2+}}$ of the material decreases by 22% compared to −1.5 A. At this point, the flow cell started to heat up significantly, and the high temperature inside the cell caused the hydrophobic layer of the GDE to fail, leading to electrolyte leakage from the anode cell into the cathode cell and interrupting the test (Figure S7a). In view of the fact that it is difficult to fully utilize the performance of a catalyst without a suitable reaction environment, in this study, the reaction cell was replaced by a carbon-doped titanium-based (Ti−C) MEA electrolytic cell with a higher mass transfer efficiency and better heat dissipation performance. The performance of electrocatalytic reduction of CCFS with $Ag_{x\%}$-pCuO was evaluated in the current range of −1 to −4 A and in a 1 M KOH electrolyte. The test results show that $Ag_{x\%}$-pCuO exhibits a lower response potential under the same current density in the test environment described above (Figure S8). Additionally, no significant heating was observed in the MEA cell during the experiment, indicating that this test environment is suitable for medium-scale testing of $Ag_{x\%}$-pCuO. As shown in Figure 4a, $Ag_{0.875\%}$-pCuO still maintains an extremely superior C_{2+} faradic efficiency of 94% at high currents up to −4 A, whereas pCuO is only able to obtain a peak 81.5% faradic efficiency for the C_{2+} product at relatively small currents. When the applied current rose to −4 A, its $FE_{C_{2+}}$ had already decreased to 66% (Figure 4b), which indicated that a portion of the active site of the undoped Ag-doped pCuO was deactivated under high currents, which could be caused by the easy reconfiguration of pCuO under the strong reducing conditions of high currents.[47] In contrast, the high current tolerance of $Ag_{0.875\%}$-pCuO may be attributed to the fact that the Cu−Ag sites formed upon the introduction of Ag are capable of both stabilizing the valence state of Cu^{2+} on the surface of the material and its coordination environment, as well as acting as a catalytically active site in the CORR. Additionally, the performance of $Ag_{0.875\%}$-pCuO at −4 A is far ahead of other ratio of Ag doping (Figures 4c and S7b−d), suggesting that $Ag_{0.875\%}$-pCuO has the best Ag:Cu ratio. It is also worth mentioning that the small amount of Ag doping greatly enhances the reaction potential window of the material, and only when the doping amount of Ag is higher than 1.25% is the $FE_{C_{2+}}$ of the material at −4 A lower than that of pCuO. Considering that AgNps are formed when the doping amount of Ag is higher than 1%, the present study speculates that a small amount of Ag doping can form Cu−Ag active sites on the surface of pCuO and, at the same time, avoid the aggregation of too much Ag to form AgNps to destroy the surface structure, which can improve the catalytic performance of the catalysts under high currents. In addition, it has been demonstrated that AgNps also inhibit the selectivity of the catalyst for C_{2+} products.[37]

In order to verify that $Ag_{0.875\%}$-pCuO is able to efficiently reduce the CCFS over a long period of time, the present study was carried out in a 1 M KOH electrolyte, with a simulated configuration of CCFS according to the current composition of the flue gas in the calcium carbide furnace industry (85% CO + 10% CO_2 + 5%N_2). Chronopotentiometry stability tests were carried out under simulated CCFS compositions at a constant current of −4 A for a long period of time, and the products were collected at regular intervals for analysis. Ultimately, $Ag_{0.875\%}$-pCuO was able to achieve a stable operation for about 110 h with its operating voltage always maintained at −3.4 ± 0.1 V, and the $FE_{C_{2+}}$ (84.77%) after 110 h of reaction was only attenuated by about 6.08% compared with that at the beginning of the reaction (90.85%), which demonstrated excellent −4 A durability (Figure 4e). In contrast, the catalytic performance of pCuO starts to drop off a cliff after 4 h of reaction under the same test conditions ($FE_{C_{2+}} \approx 46.9\%$), and the operating voltage of pCuO (−4.8 V) is much higher than that of $Ag_{0.875\%}$-pCuO (Figure S9). This suggests that the introduction of Ag improves the stability of the catalyst in treating simulated CCFS under high currents and reduces the treatment energy consumption, reflecting the excellent potential of $Ag_{0.875\%}$-pCuO in the field of industrial-scale resourcefulness of CCFS. Finally, this study preliminarily explored the model of $Ag_{0.875\%}$-pCuO for industrial applications and achieved CORR tests in simulated CCFS as well as at −8 A by connecting two MEA cell bodies in parallel and obtained 81.05% of the C_{2+} faradic efficiency and nearly double the amount of product compared to a single MEA cell at −4 A. (Figures S10 and S11)

https://doi.org/10.1021/acsenvironau.4c00121
ACS Environ. Au 2025, 5, 287−297

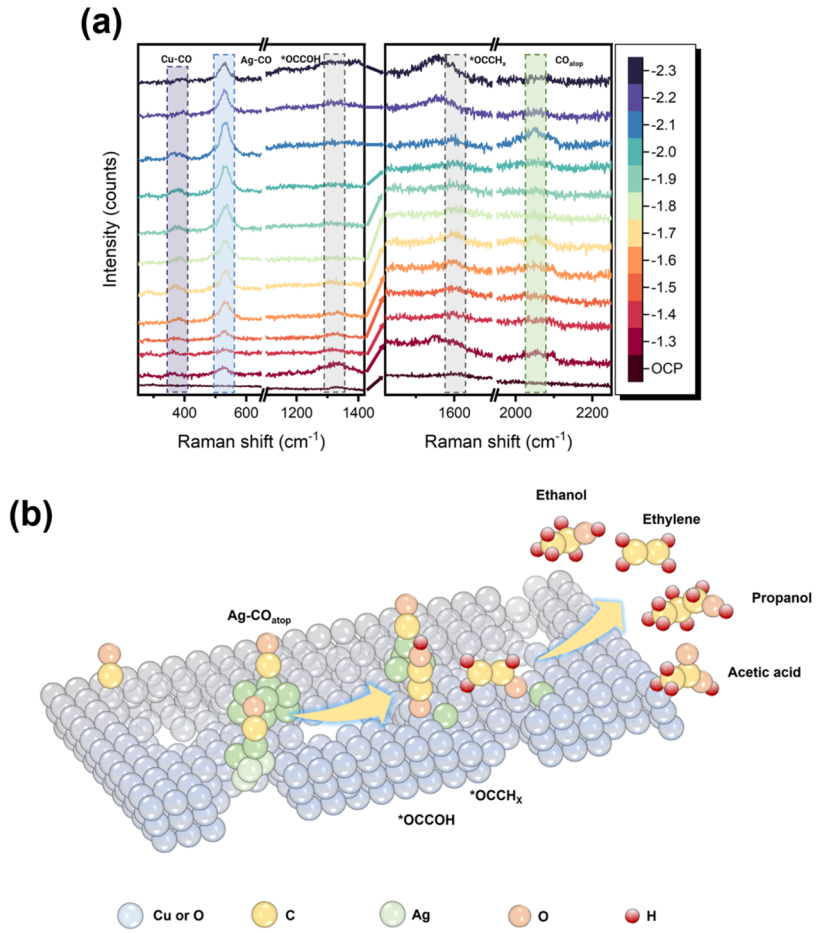

Figure 6. (a) In situ Raman spectroscopy studies of $Ag_{0.875\%}$-pCuO in a flow cell with the electrodes in contact with 1 M KOH; (b) schematic illustration of the possible reaction pathway of CO reduction over $Ag_{0.875\%}$-pCuO.

In Situ and Post Catalysis Characterizations

To preliminarily investigate the effect of Ag doping on the surface valence stability of the materials, our team performed XPS tests on $Ag_{0.875\%}$-pCuO after 110 h of reaction and on pCuO after 4.5 h of reaction. Since the peak positions of CuO $2p_{3/2}$ (933.6 eV) and Cu_2O $2p_{3/2}$ (932.8 eV) in the XPS energy spectrum of Cu 2p are too close to be analyzed (Figure S12), the present study found that the surface valence state of $Ag_{0.875\%}$-pCuO after the reaction for 110 h was mainly Cu^{2+} (569.2 eV) with a small amount of Cu^+ (573.1 eV) after 110 h of reaction,[48] suggesting that the catalyst has good valence stability with only a small portion of the catalyst undergoing in situ reduction during the treatment of simulated CCFS (Figure 5a). In contrast, pCuO obviously possesses a stronger peak at 573.1 eV (Cu^+), which suggests that the doping of Ag can improve the valence stability of Cu in the treatment of simulated gas, which lays the foundation for its ability to stably and efficiently resource the flue gas of a calcium carbide furnace (Figure 5b).

Then, in order to further investigate the mechanism of doping the appropriate amount of Ag in pCuO to improve the catalyst processing performance, this study was carried out to identify the different intermediates and surface substances produced during the electrocatalytic reduction of simulated CCFS by $Ag_{0.875\%}$-pCuO and pCuO using in situ Raman. To distinguish between intermediates and surface species with similar peak positions, a curve-fitting method was employed in this study to analyze the regions where peak overlap occurs (Figure S14). For $Ag_{0.875\%}$-pCuO, it was found that the Cu-CO stretching peak (380 cm^{-1}) gradually disappeared with the increase of applied potential, while the Ag-CO peak (535 cm^{-1}) first strengthened and then weakened and had a very strong peak signal at −2.0 V. This indicates that the main CO adsorption site changed from Cu to Ag under high current and enhanced the CO adsorption on the catalyst surface. Meanwhile, the Cu-*OH peak (520 cm^{-1}) exhibited a tendency to weaken initially and then strengthen as the applied potential increased. Considering that *OH can serve as a carrier of both electrons and protons on the catalyst surface,[49] we conclude that $Ag_{0.875\%}$-pCuO enhances the hydrogenation efficiency of C_{2+} intermediates at medium to high potentials and demonstrates excellent electron transfer capability. In addition, the *OCCOH peak (1310 cm^{-1}) was also observed at low potentials as well as the *$OCCH_x$ peak (1610 cm^{-1}) at medium to high potentials.[50] The former is a key intermediate for the formation of ethanol and propanol, while the latter is a key intermediate for the formation of acetic acid, which suggests that $Ag_{0.875\%}$-pCuO is more inclined to generate ethanol and propanol at small currents and more selective for acetic acid at large currents, and this analysis is also in agreement with the results of the performance test of $Ag_{0.875\%}$-pCuO in a simulated CCFS atmosphere (Figure 6a). In contrast, pCuO has strong Cu-CO stretching, and CO_{atop} (2065 cm^{-1}) peaks only at low potentials, and the signal of the Cu−OH peak (520 cm^{-1}) is gradually enhanced with

https://doi.org/10.1021/acsenvironau.4c00121
ACS Environ. Au 2025, 5, 287−297

increasing potential, which suggests that pCuO reduces the adsorption of CO at high potentials, thereby lowering the rate of *OH consumption (Figure S13). In summary, the introduction of Ag improves the adsorption of CO by CuO at high currents and provides abundant Cu−Ag sites to optimize the C_{2+} selectivity of CuO (Figure 6b).

CONCLUSIONS

This study presents a CORR technology that achieves high C_{2+} faradic efficiencies at elevated currents, utilizing a porous CuO catalyst with 0.875% Ag doping. This technology demonstrates significant potential for the efficient resource utilization of CCFS. $Ag_{0.875\%}$-pCuO demonstrated stable and efficient electrocatalytic reduction of simulated CCFS in a Ti−C MEA electrolytic cell at a high current of −4 A. It achieved a high C_{2+} faradic efficiency of up to 94% and maintained over 84% efficiency after 110 h of operation. The superior CORR performance of $Ag_{0.875\%}$-pCuO in a simulated CCFS atmosphere is attributed to moderate Ag doping, which enhances the porous CuO by providing selective Cu−Ag active sites, increasing the CO coverage, and stabilizing the valence of CuO. These effects are strongly supported by both ex situ characterization and in situ Raman testing. Finally, this study conducted CORR tests using two parallelly connected MEA cells under simulated CCFS and at −8 A, achieving an 81.05% C_{2+} faradic efficiency and nearly double the product yield compared to a single MEA cell at −4 A. This work fills a technological gap in the utilization of CORR for the recovery of CO-containing industrial flue gases, providing valuable insights that will undeniably illuminate novel possibilities for the industrial application of the CORR.

ASSOCIATED CONTENT

Supporting Information

The Supporting Information is available free of charge at https://pubs.acs.org/doi/10.1021/acsenvironau.4c00121.

The composition of calcium carbide furnace flue gas; summary of catalyst current density, C_{2+} faradic efficiency, and catalyst stability indices for relevant copper-based catalysts; $Ag_{x\%}$-pCuO EDS data; and BET analysis data of $Ag_{x\%}$-pCuO (Tables S1−S4); SEM images of other $Ag_{x\%}$-pCuO; TEM images of other $Ag_{x\%}$-pCuO; element mapping analyses for $Ag_{0.75\%}$-pCuO and $Ag_{1\%}$-pCuO; particle size histograms of the $Ag_{0.875\%}$-pCuO; XPS patterns of other $Ag_{x\%}$-pCuO; electrocatalytic performances of the $Ag_{x\%}$-pCuO for CORR at −1.4 A; electrocatalytic CORR performance of $Ag_{0.875\%}$-pCuO tested in a flow cell on a laboratory scale and FE distribution of the CORR products for the other Ag $_{x\%}$-pCuO in a MEA cell; current density and response potential of $Ag_{x\%}$-CuO in all tests; chronopotentiometry stability test of pCuO at −4 A in MEA; schematic diagram of a MEA double-cell parallel system; voltage plot of MEA double-cell parallel system at −8 A and simulated CCFS; XPS patterns of $Ag_{0.875\%}$-pCuO after the 110 h CORR reaction; in situ Raman spectroscopy studies of pCuO; and in situ Raman spectroscopy of $Ag_{0.875\%}$-pCuO at 475−575 cm^{-1} for curve fitting (Figures S1−S14) (PDF)

AUTHOR INFORMATION

Corresponding Author

Wenlei Zhu − *State Key Laboratory of Pollution Control and Resource Reuse, State Key Laboratory of Analytical Chemistry for Life Science, the Frontiers Science Center for Critical Earth Material Cycling, School of the Environment, School of Chemistry and Chemical Engineering, Nanjing University, Nanjing 210023, China;* orcid.org/0000-0001-6110-993X; Email: wenleizhu@nju.edu.cn

Authors

Zhengkai Zhuang − *State Key Laboratory of Pollution Control and Resource Reuse, State Key Laboratory of Analytical Chemistry for Life Science, the Frontiers Science Center for Critical Earth Material Cycling, School of the Environment, School of Chemistry and Chemical Engineering, Nanjing University, Nanjing 210023, China*

Guangtao Wang − *State Key Laboratory of Pollution Control and Resource Reuse, State Key Laboratory of Analytical Chemistry for Life Science, the Frontiers Science Center for Critical Earth Material Cycling, School of the Environment, School of Chemistry and Chemical Engineering, Nanjing University, Nanjing 210023, China*

Wen Zhao − *State Key Laboratory of Pollution Control and Resource Reuse, State Key Laboratory of Analytical Chemistry for Life Science, the Frontiers Science Center for Critical Earth Material Cycling, School of the Environment, School of Chemistry and Chemical Engineering, Nanjing University, Nanjing 210023, China*

Ruixin Yang − *State Key Laboratory of Pollution Control and Resource Reuse, State Key Laboratory of Analytical Chemistry for Life Science, the Frontiers Science Center for Critical Earth Material Cycling, School of the Environment, School of Chemistry and Chemical Engineering, Nanjing University, Nanjing 210023, China*

Yilin Zhou − *Nanjing No.1 High School, Nanjing 210000, China*

Complete contact information is available at: https://pubs.acs.org/10.1021/acsenvironau.4c00121

Author Contributions

CRediT: **Zhengkai Zhuang** conceptualization, data curation; **Guangtao Wang** data curation, formal analysis; **Wen Zhao** formal analysis; **Ruixin Yang** writing - original draft; **Yilin Zhou** software; **Wenlei Zhu** funding acquisition, project administration.

Notes

The authors declare no competing financial interest.

ACKNOWLEDGMENTS

The authors would like to acknowledge the support from the National Natural Science Foundation of China (22176086), Research Funds for Jiangsu Distinguished Professor, Carbon Peaking and Carbon Neutrality Technological Innovation Foundation of Jiangsu Province (BE2022861), the Research Funds from Frontiers Science Center for Critical Earth Material Cycling of Nanjing University (021114380217), State Key Laboratory of Pollution Control and Resource Reuse, and the Fundamental Research Funds for the Central Universities (021114380214 and 021114380222).

REFERENCES

(1) Wang, X.; Ou, P. F.; Ozden, A.; Hung, S. F.; Tam, J.; Gabardo, C. M.; Howe, J. Y.; Sisler, J.; Bertens, K.; de Arquer, F. P. G.; et al. Efficient electrosynthesis of *n*-propanol from carbon monoxide using a Ag-Ru-Cu catalyst. *Nat. Energy* **2022**, *7* (2), 170−176.

(2) Liu, J.; Burciaga, R.; Tang, S.; Ding, S.; Ran, H.; Zhao, W.; Wang, G.; Zhuang, Z.; Xie, L.; Lyu, Z.; et al. Heterogeneous catalysis for the environment. *Innov. Mater.* **2024**, *2* (3), No. 100090.

(3) Fu, J.; Li, P.; Lin, Y.; Du, H.; Liu, H.; Zhu, W.; Ren, H. Fight for carbon neutrality with state-of-the-art negative carbon emission technologies. *Eco-Environ. Health* **2022**, *1* (4), 259−279.

(4) Johnson, D.; Pranada, E.; Yoo, R.; Uwadiunor, E.; Ngozichukwu, B.; Djire, A. Review and Perspective on Transition Metal Electrocatalysts Toward Carbon-Neutral Energy. *Energy Fuels* **2023**, *37* (3), 1545−1576.

(5) Kar, S.; Sen, R.; Goeppert, A.; Prakash, G. K. S. Integrative CO_2 Capture and Hydrogenation to Methanol with Reusable Catalyst and Amine: Toward a Carbon Neutral Methanol Economy. *J. Am. Chem. Soc.* **2018**, *140* (5), 1580−1583.

(6) Olah, G. A.; Goeppert, A.; Prakash, G. K. S. Chemical Recycling of Carbon Dioxide to Methanol and Dimethyl Ether: From Greenhouse Gas to Renewable, Environmentally Carbon Neutral Fuels and Synthetic Hydrocarbons. *J. Org. Chem.* **2009**, *74* (2), 487−498.

(7) Hu, Y.; Ding, Y.; Xie, L.; Li, H.; Jiang, Y.; Gong, K.; Zhang, A.; Zhu, W.; Wang, Y. Carbon-based materials for low concentration CO_2 capture and electrocatalytic reduction. *Carbon* **2024**, *230*, No. 119574.

(8) Yang, R.; Cai, Y.; Qi, Y.; Tang, Z.; Zhu, J.-J.; Li, J.; Zhu, W.; Chen, Z. How local electric field regulates C−C coupling at a single nanocavity in electrocatalytic CO_2 reduction. *Nat. Commun.* **2024**, *15* (1), No. 7140.

(9) Cai, Y.; Yang, R.; Fu, J.; Li, Z.; Xie, L.; Li, K.; Chang, Y.-C.; Ding, S.; Lyu, Z.; Zhang, J.-R.; et al. Self-pressurizing nanoscale capsule catalysts for CO_2 electroreduction to acetate or propanol. *Nat. Synth.* **2024**, *3* (7), 891−902.

(10) Du, H. T.; Liu, L. X.; Li, P.; Min, Q. H.; Guo, S. J.; Zhu, W. L. Enriching Reaction Intermediates in Multishell Structured Copper Catalysts for Boosted Propanol Electrosynthesis from Carbon Monoxide. *ACS Nano* **2023**, *17* (9), 8663−8670.

(11) Du, H. T.; Liu, L. X.; Cai, Y. M.; Wang, Y.; Zhang, J. R.; Min, Q. H.; Zhu, W. L. *In situ* formed N-containing copper nanoparticles: a high-performance catalyst toward carbon monoxide electroreduction to multicarbon products with high faradaic efficiency and current density. *Nanoscale* **2022**, *14* (19), 7262−7268.

(12) Rabiee, H.; Ge, L.; Zhang, X. Q.; Hu, S. H.; Li, M. R.; Yuan, Z. G. Gas diffusion electrodes (GDEs) for electrochemical reduction of carbon dioxide, carbon monoxide, and dinitrogen to value-added products: a review. *Energy Environ. Sci.* **2021**, *14* (4), 1959−2008.

(13) Liu, Z. National carbon emissions from the industry process: Production of glass, soda ash, ammonia, calcium carbide and alumina. *Appl. Energy* **2016**, *166*, 239−244.

(14) Jouny, M.; Hutchings, G. S.; Jiao, F. Carbon monoxide electroreduction as an emerging platform for carbon utilization. *Nat. Catal.* **2019**, *2* (12), 1062−1070.

(15) Jiang, M.; Wang, Z.-H.; Ning, P.; Tian, S.-L.; Huang, X.-F.; Bai, Y.-W.; Shi, Y.; Ren, X.-G.; Chen, W.; Qin, Y.-S.; et al. Dust removal and purification of calcium carbide furnace off-gas. *J. Taiwan Inst. Chem. Eng.* **2014**, *45* (3), 901−907.

(16) Mi, Y.; Zheng, D. X.; Jiang, X. Z. Multi-product carbon footprint assessment for low-rank coal-based acetylene manufacturing process. *J. Cleaner Prod.* **2016**, *112*, 1676−1682.

(17) Ni, M.; Leung, D. Y. C.; Leung, M. K. H.; Sumathy, K. An overview of hydrogen production from biomass. *Fuel Process. Technol.* **2006**, *87* (5), 461−472.

(18) Wu, N.; Geng, G.; Qin, X.; Tong, D.; Zheng, Y.; Lei, Y.; Zhang, Q. Daily Emission Patterns of Coal-Fired Power Plants in China Based on Multisource Data Fusion. *ACS Environ. Au* **2022**, *2* (4), 363−372.

(19) Liu, X. Y.; Zhu, B.; Zhou, W. J.; Hu, S. Y.; Chen, D. J.; Griffy-Brown, C. CO_2 emissions in calcium carbide industry: An analysis of China's mitigation potential. *Int. J. Greenhouse Gas Control* **2011**, *5* (5), 1240−1249.

(20) Jiang, L. L.; Meng, Y. M.; Zhang, W. P.; Yu, H. T.; Hou, X. G. Preparation of NH_2-SH-GO/SWCNTs based on graphene oxide/single-walled carbon nanotubes for CO_2 and N_2 separation from blast furnace gas. *Microporous Mesoporous Mater.* **2020**, *306*, No. 110476.

(21) Jouny, M.; Luc, W.; Jiao, F. High-rate electroreduction of carbon monoxide to multi-carbon products. *Nat. Catal.* **2018**, *1* (10), 748−755.

(22) Wang, X. Y.; Chen, Y. J.; Li, F.; Miao, R. K.; Huang, J. E.; Zhao, Z. L.; Li, X. Y.; Dorakhan, R.; Chu, S. L.; Wu, J. H.; et al. Site-selective protonation enables efficient carbon monoxide electroreduction to acetate. *Nat. Commun.* **2024**, *15* (1), No. 616.

(23) Li, C. W.; Ciston, J.; Kanan, M. W. Electroreduction of carbon monoxide to liquid fuel on oxide-derived nanocrystalline copper. *Nature* **2014**, *508* (7497), 504−507.

(24) Zhao, W.; Liu, J.; Wang, G. T.; Wang, X. T.; Yang, C. J.; Li, J.; Wang, Y. T.; Sun, X. L.; Lin, R. C.; Zuo, G. C.; Zhu, W. Copper-based catalysts for carbon monoxide electroreduction to multi-carbon products. *Sci. China: Mater.* **2024**, *67* (6), 1684−1705.

(25) Bao, H. H.; Qiu, Y.; Peng, X. Y.; Wang, J. A.; Mi, Y. Y.; Zhao, S. Z.; Liu, X. J.; Liu, Y. F.; Cao, R.; Zhuo, L. C.; et al. Isolated copper single sites for high-performance electroreduction of carbon monoxide to multicarbon products. *Nat. Commun.* **2021**, *12* (1), No. 238.

(26) Li, S.; Guan, A. X.; Yang, C.; Peng, C.; Lv, X. M.; Ji, Y. L.; Quan, Y. L.; Wang, Q. H.; Zhang, L. J.; Zheng, G. F. Dual-Atomic Cu Sites for Electrocatalytic CO Reduction to C_{2+} Products. *ACS Mater. Lett.* **2021**, *3* (12), 1729−1737.

(27) Guan, A. X.; Wang, Q. H.; Ji, Y. L.; Li, S.; Yang, C.; Qian, L. P.; Zhang, L. J.; Wu, L. M.; Zheng, G. F. Steric effect induces CO electroreduction to CH_4 on Cu-Au alloys. *J. Mater. Chem. A* **2021**, *9* (38), 21779−21784.

(28) Luc, W.; Fu, X.; Shi, J.; Lv, J.-J.; Jouny, M.; Ko, B. H.; Xu, Y.; Tu, Q.; Hu, X.; Wu, J.; Yue, Q.; Liu, Y.; Jiao, F.; Kang, Y. Two-dimensional copper nanosheets for electrochemical reduction of carbon monoxide to acetat. *Nature Catalysis* **2019**, *2*, 423−430.

(29) Nitopi, S.; Bertheussen, E.; Scott, S. B.; Liu, X. Y.; Engstfeld, A. K.; Horch, S.; Seger, B.; Stephens, I. E. L.; Chan, K.; Hahn, C.; et al. Progress and Perspectives of Electrochemical CO_2 Reduction on Copper in Aqueous Electrolyte. *Chem. Rev.* **2019**, *119* (12), 7610−7672.

(30) Xie, L. Y. Q.; Jiang, Y. J.; Zhu, W. L.; Ding, S. C.; Zhou, Y.; Zhu, J. J. Cu-based catalyst designs in CO_2 electroreduction: precise modulation of reaction intermediates for high-value chemical generation. *Chem. Sci.* **2023**, *14* (47), 13629−13660.

(31) Liu, L. X.; Li, X.; Cai, Y. M.; Du, H. T.; Liu, F. Q.; Zhang, J. R.; Fu, J. J.; Zhu, W. L. Hierarchical S-modified Cu porous nanoflakes for efficient CO_2 electroreduction to formate. *Nanoscale* **2022**, *14* (37), 13679−13688.

(32) Ji, Y.; Yang, C.; Qian, L.; Zhang, L.; Zheng, G. Promoting electrocatalytic carbon monoxide reduction to ethylene on copper-polypyrrole interface. *J. Colloid Interface Sci.* **2021**, *600*, 847−853.

(33) Zhuang, T. T.; Pang, Y. J.; Liang, Z. Q.; Wang, Z. Y.; Li, Y.; Tan, C. S.; Li, J.; Dinh, C. T.; De Luna, P.; Hsieh, P. L.; et al. Copper nanocavities confine intermediates for efficient electrosynthesis of C_3 alcohol fuels from carbon monoxide. *Nat. Catal.* **2018**, *1* (12), 946−951.

(34) Du, H. T.; Fu, J. J.; Liu, L. X.; Ding, S. C.; Lyu, Z.; Jin, X.; Kengara, F. O.; Song, B.; Min, Q. H.; Zhu, J. J.; et al. Recent progress in electrochemical reduction of carbon monoxide toward multi-carbon products. *Mater. Today* **2022**, *59*, 182−199.

(35) Long, C.; Wan, K. W.; Chen, Y.; Li, L.; Jiang, Y. H.; Yang, C. Y.; Wu, Q. B.; Wu, G. L.; Xu, P.; Li, J.; et al. Steering the Reconstruction of Oxide-Derived Cu by Secondary Metal for Electrosynthesis of *n*-Propanol from CO. *J. Am. Chem. Soc.* **2024**, *146* (7), 4632−4641.

https://doi.org/10.1021/acsenvironau.4c00121
ACS Environ. Au 2025, 5, 287−297

(36) Dorakhan, R.; Grigioni, I.; Lee, B. H.; Ou, P. F.; Abed, J.; O'Brien, C.; Rasouli, A. S.; Plodinec, M.; Miao, R. K.; Shirzadi, E.; et al. A silver-copper oxide catalyst for acetate electrosynthesis from carbon monoxide. *Nat. Synth.* **2023**, *2* (5), 448−457.
(37) Nørskov, J. K.; Bligaard, T.; Logadottir, A.; Kitchin, J. R.; Chen, J. G.; Pandelov, S.; Norskov, J. K. Trends in the exchange current for hydrogen evolution. *J. Electrochem. Soc.* **2005**, *152* (3), J23−J26.
(38) Zhang, Y. J.; Sethuraman, V.; Michalsky, R.; Peterson, A. A. Competition between CO_2 Reduction and H_2 Evolution on Transition-Metal Electrocatalysts. *ACS Catal.* **2014**, *4* (10), 3742−3748.
(39) Jiang, P.; Zhao, G. H.; Zhang, H.; Ji, T.; Mu, L. W.; Lu, X. H.; Zhu, J. H. Towards carbon neutrality of calcium carbide-based acetylene production with sustainable biomass resources. *Green Energy Environ.* **2024**, *9* (6), 1068−1078.
(40) Phetchuay, C.; Horpibulsuk, S.; Arulrajah, A.; Suksiripattanapong, C.; Udomchai, A. Strength development in soft marine clay stabilized by fly ash and calcium carbide residue based geopolymer. *Appl. Clay Sci.* **2016**, *127*−*128*, 134−142.
(41) Brown, P. N.; Jayson, G. G.; Thompson, G.; Wilkinson, M. C. Adsorption Characteristics of Impregnated Activated-Charcoal Cloth for Hydrogen-Cyanide. *J. Colloid Interface Sci.* **1987**, *116* (1), 211−220.
(42) Zhao, H. B.; Tonkyn, R. G.; Barlow, S. E.; Peden, C. H. F.; Koel, B. E. Fractional factorial study of HCN removal over a 0.5% Pt/Al_2O_3 catalyst:: Effects of temperature, gas flow rate, and reactant partial pressure. *Ind. Eng. Chem. Res.* **2006**, *45* (3), 934−939.
(43) Lv, J. J.; Jouny, M.; Luc, W.; Zhu, W. L.; Zhu, J. J.; Jiao, F. A Highly Porous Copper Electrocatalyst for Carbon Dioxide Reduction. *Adv. Mater.* **2018**, *30* (49), No. 1803111, DOI: 10.1002/adma.201803111.
(44) Zhang, W.; Zhu, N.; Ding, L.; Hu, Y.; Wu, Z. Efficacious CO_2 Adsorption and Activation on Ag Nanoparticles/CuO Mesoporous Nanosheets Heterostructure for CO_2 Electroreduction to CO. *Inorg. Chem.* **2021**, *60* (24), 19356−19364.
(45) Zhang, W. Z. Z.; Zhu, N. N.; Ding, L. C.; Hu, Y.; Wu, Z. C. Efficacious CO_2 Adsorption and Activation on Ag Nanoparticles/CuO Mesoporous Nanosheets Heterostructure for CO_2 Electroreduction to CO. *Inorg. Chem.* **2021**, *60* (24), 19356−19364.
(46) He, S. S.; Ni, F. L.; Ji, Y. J.; Wang, L. E.; Wen, Y. Z.; Bai, H. P.; Liu, G. J.; Zhang, Y.; Li, Y. Y.; Zhang, B.; Peng, H. The p-Orbital Delocalization of Main-Group Metals to Boost CO_2 Electroreduction. *Angew. Chem., Int. Ed.* **2018**, *57* (49), 16114−16119.
(47) Lee, S.; Kim, D.; Lee, J. Electrocatalytic Production of C_3-C_4 Compounds by Conversion of CO_2 on a Chloride-Induced Bi-Phasic Cu_2O-Cu Catalyst. *Angew. Chem., Int. Ed.* **2015**, *54* (49), 14701−14705.
(48) Wang, L.; Nitopi, S.; Wong, A. B.; Snider, J. L.; Nielander, A. C.; Morales-Guio, C. G.; Orazov, M.; Higgins, D. C.; Hahn, C.; Jaramillo, T. F. Electrochemically converting carbon monoxide to liquid fuels by directing selectivity with electrode surface area. *Nat. Catal.* **2019**, *2* (8), 702−708.
(49) Gorthy, S.; Verma, S.; Sinha, N.; Shetty, S.; Nguyen, H.; Neurock, M. Theoretical Insights into the Effects of KOH Concentration and the Role of OH− in the Electrocatalytic Reduction of CO2 on Au. *ACS Catal.* **2023**, *13* (19), 12924−12940.
(50) Luan, P.; Dong, X.; Liu, L. Q.; Xiao, J. P.; Zhang, P. F.; Zhang, J.; Chi, H. B.; Wang, Q. N.; Ding, C. M.; Li, R. G.; Li, C. Selective Electrosynthesis of Ethanol via Asymmetric C-C Coupling in Tandem CO2 Reduction. *ACS Catal.* **2024**, *14* (11), 8776−8785.

https://doi.org/10.1021/acsenvironau.4c00121
ACS Environ. Au 2025, 5, 287−297